Molecular Cancer Therapeutics

MORAb-202, an Antibody–Drug Conjugate Utilizing Humanized Anti-human FRα Farletuzumab and the Microtubule-targeting Agent Eribulin, has Potent Antitumor Activity

Xin Cheng[1], Jing Li[2], Keigo Tanaka[3], Utpal Majumder[4], Andrew Z. Milinichik[1], Arielle C. Verdi[1], Christopher J. Maddage[5], Katherine A. Rybinski[5], Shawn Fernando[6], Danielle Fernando[6], Megan Kuc[6], Keiji Furuuchi[5], Frank Fang[2], Toshimitsu Uenaka[5], Luigi Grasso[7], and Earl F. Albone[1]

Abstract

Microtubule-targeting agents (MTA) have been investigated for many years as payloads for antibody–drug conjugates (ADC). In many cases, these ADCs have shown limited benefits due to lack of efficacy or significant toxicity, which has spurred continued investigation into novel MTA payloads for next-generation ADCs. In this study, we have developed ADCs using the MTA eribulin, a derivative of the macrocyclic polyether natural product halichondrin B, as a payload. Eribulin ADCs demonstrated *in vitro* potency and specificity using various linkers and two different conjugation approaches. MORAb-202 is an investigational agent that consists of the humanized anti-human folate receptor alpha (FRA) antibody farletuzumab conjugated via reduced interchain disulfide bonds to maleimido-PEG_2-valine-citrulline-*p*-aminobenzylcarbamyl-eribulin at a drug-to-antibody ratio of 4.0. MORAb-202 displayed preferable biophysical properties and broad potency across a number of FRA-positive tumor cell lines as well as demonstrated improved specificity *in vitro* compared with farletuzumab conjugated with a number of other MTA payloads, including MMAE, MMAF, and the reducible maytansine linker-payload sulfo-SPDB-DM4. A single-dose administration of MORAb-202 in FRA-positive human tumor cell line xenograft and patient-derived tumor xenograft models elicited a robust and durable antitumor response. These data support further investigation of MORAb-202 as a potential new treatment modality for FRA-positive cancers, using the novel MTA eribulin as a payload. *Mol Cancer Ther; 17(12); 2665–75. ©2018 AACR.*

Introduction

Microtubules, which consist of heterodimers of α- and β-tubulin assembled into a dynamic polymeric structure, are involved in many cellular processes critical to proper cell function and survival, including mitosis, cell migration, and vesicle and organelle transport (1, 2). When the process of coordinated microtubule assembly and disassembly is disrupted, cells are arrested in G_2–M phase and enter apoptosis, ultimately leading to cell death. Thus, microtubule-targeting agents (MTA) have long been investigated, and used clinically in some cases, for the treatment of cancer (3–5). Typically, MTAs fall into two classes: (i) those that stabilize the microtubule assembly and promote the polymerization of growing microtubules, and (ii) those that disrupt formed microtubules and promote microtubule disassembly. Examples of microtubule-stabilizing MTAs are the taxanes, including docetaxel and paclitaxel, and examples of microtubule polymerization inhibitors/depolymerization promoters include dolastatins, cryptophycins, halichondrins, maytansines, and vinblastine. While some MTAs have been approved for use as chemotherapeutics and are widely used in the clinics, including paclitaxel and vinblastine, toxicity has limited the use of certain MTAs as chemotherapeutic agents (6–8). However, the high potency of many of these compounds (IC_{50}: 10^{-9} mol/L to $<10^{-11}$ mol/L) makes them attractive candidates as payloads in antibody–drug conjugates (ADC) for targeted therapy of cancer.

A number of classes of MTAs have been investigated as payloads for ADCs and in some cases approved for clinical use. For example, the highly potent synthetic derivatives of the natural product dolastatin auristatin E, auristatin F, and their monomethyl derivatives (MMAE and MMAF, respectively) have been widely explored as payloads and, in some instances, the resulting ADCs are currently being investigated in clinical trials

[1]Department of Biochemistry Discovery, Oncology Biologics Laboratories, Oncology Business Group, Eisai Inc, Exton, Pennsylvania. [2]Department of Translational Chemistry, Eisai AiM Institute, Eisai Inc., Andover, Massachusetts. [3]Department of Chemistry Research, Eisai Co. Ltd., Tsukuba-Shi, Ibaraki, Japan. [4]Department of Discovery Chemistry, Eisai AiM Institute, Eisai Inc., Andover, Massachusetts. [5]Department of Preclinical Development, Oncology Biologics Laboratories, Oncology Business Group, Eisai Inc, Exton, Pennsylvania. [6]Department of Bioanalytical Development, Oncology Biologics Laboratories, Oncology Business Group, Eisai Inc, Exton, Pennsylvania. [7]Department of Discovery Research, Morphotek Inc., Exton, Pennsylvania.

Note: Supplementary data for this article are available at Molecular Cancer Therapeutics Online (http://mct.aacrjournals.org/).

Corresponding Author: Earl F. Albone, Department of Biochemistry Discovery, Oncology Biologics Laboratories, Oncology Business Group, Eisai, Inc, 210 Welsh Pool Rd, Exton, PA 19341. Phone: 610-423-6138; Fax 610-423-6120; E-mail: ealbone@morphotek.com

doi: 10.1158/1535-7163.MCT-17-1215

(9). Brentuximab vedotin (Adcetris) consisting of monomethyl auristatin E conjugated to mouse-human chimeric anti-human CD30 cAC10 via a cathepsin-cleavable valine-citruline (Val-Cit) chemical linker is approved in the United States for the treatment of relapsed Hodgkin lymphoma and systemic anaplastic large-cell lymphoma (sALCL; ref. 10). Maytansines, including the derivatives DM1 and DM4, are also widely used as payloads for ADCs. DM1, linked via a noncleavable SMCC to trastuzumab, is approved for treatment of patients with HER2-positive ($HER2^+$), metastatic breast cancer who previously received trastuzumab and a taxane (11). However, ADCs using current MTAs as payloads have, in many cases, suffered from lack of efficacy and/or problematic toxicities. Clinically, both maytansine- and auristatin-based ADCs have demonstrated significant ocular toxicity and peripheral neuropathy, which in many cases has resulted in treatment discontinuation or dose reduction. These results clearly demonstrate that, in addition to continued research into new linker modalities and novel antibody targets for ADCs using existing MTA payloads, there is a need to continue to investigate other cytotoxic agents and MTAs as payloads for ADCs that may provide reduced toxicities and/or improved therapeutic index.

Eribulin is a synthetic analogue of the macrocyclic polyether halichondrin B, which was originally isolated from the Asian sea sponge *Halichondria okadai* (12). Eribulin binds specifically to the β-tubulin subunit on the (+) end of the microtubule and potently inhibits elongation of the formed microtubule, while having little or no effect on microtubule depolymerization (13). At higher concentrations, eribulin promotes the formation of nonfunctional drug–tubulin dimer species. Eribulin mesylate, marketed as Halaven, is approved in the United States for the treatment of metastatic breast cancer in patients who have received at least two prior treatment regimens that include an anthracycline and a taxane (14). In addition to its antimitotic effects, eribulin has also been demonstrated to have significant nonmitotic effects, which may contribute to its overall antitumor activity. Eribulin has been shown to inhibit cancer cell migration (15), increase tumor perfusion leading to increased tumor oxygenation and greater tumor penetration by subsequently administered agents (16–18), decrease circulating VEGF (18), and promote a mesenchymal-to-epithelial transition in tumor phenotype (19, 20). Eribulin has also been shown to cause less peripheral neuropathy compared with other MTAs in animal models and clinically (21–23). Eribulin's potent antimitotic activity and nonmitotic effects on tumor biology make it an interesting candidate for investigation as a MTA payload for ADCs.

Folate receptor alpha (FRA) is a GPI-linked protein that has been demonstrated to be overexpressed in many tumor types, including ovarian, endometrial, lung, and triple-negative breast cancer (24–26). Farletuzumab is a humanized anti-human FRA mAb currently in clinical trials for the treatment of platinum-sensitive ovarian cancer. Farletuzumab has been shown to mediate its antitumor activity *in vivo* by inducing tumor cell autophagy in combination with immune-mediated antibody-dependent cytotoxicity (ADCC) and complement-mediated cytotoxicity (CDC; ref. 27). In a phase III clinical trial in patients with relapsed platinum-sensitive ovarian cancer plus standard-of-care, farletuzumab was shown to be safe; however, the trial did not meet its primary statistical endpoint (28). Progression-free and overall survival benefits (5 and 13 months, respectively) were observed in patients with less than three times the upper limit of normal ($\leq 3\times$ ULN) CA125 biomarker levels. This effect appeared to be due to CA125's direct binding to farletuzumab and its subsequent suppression of ADCC function (29). A confirmatory trial in patients with $\leq 3\times$ ULN CA125 is ongoing, with an expected completion date in 2019. Because of its demonstrated safety profile in the large number of patients previously treated in clinical trials and its ability to specifically target FRA-positive tumors in patients (30), farletuzumab makes an attractive targeting modality to investigate eribulin as a novel MTA payload for ADCs targeting FRA-positive cancers.

Here we demonstrate the conjugation of eribulin to mAbs using a combination of different linker and conjugation strategies. ADCs consisting of eribulin conjugated to farletuzumab are highly potent ($<10^{-10}$ mol/L) and specific (>3 logs) against FRA-positive tumor cells. One farletuzumab–eribulin conjugate, MORAb-202, comprising a self-emolative Val-Cit linker and a drug-to-antibody ratio (DAR) of 4, displayed optimal biophysical properties, potent cytotoxicity across a number of FRA-positive cell lines, and induced a robust antitumor response in mouse models of FRA-positive human cancers. These results warrant further investigation of MORAb-202 for the treatment of FRA-positive cancers and further development of eribulin-based ADCs for targeting additional tumor antigens.

Materials and Methods

Antibodies

Farletuzumab (humanized anti-human folate receptor alpha, 25 mg/mL) and amatuximab [mouse-human chimeric anti-human mesothelin (MSLN), 25 mg/mL] were of GMP grade.

Compounds

Compound stocks were prepared as 10 mmol/L in DMSO and stored at −20°C until use, unless otherwise indicated. Structures of selected compounds used in these studies are listed in Supplementary Fig. S1.

Tumor cell lines

Human tumor cell lines used in screening analyses of eribulin-based ADCs were ovarian carcinoma IGROV1, non–small cell lung cancer NCI-H2110, and epidermoid A431. Additional analyses were performed with ovarian lines OVCAR3, OVCAR3-A1, and CaOV3, gastric lines MKN7, MKN74, NCI-N87, and NUGC3, endometrial lines HEC-251, HEC-1-A, and HEC59, and the triple-negative breast cancer cell line HCC1954. Cell lines used were obtained directly from JCRB for HEC-251. MKN7, MKN74, and NUGC3 were kind gifts from Professor Sasaki at Showa University School of Medicine, Japan. IGROV1 was obtained from the National Cancer Institute, with permission. All other cell lines were obtained from ATCC. All lines were cultured in complete RPMI, unless otherwise indicated. All cell lines were tested for *Mycoplasma* upon receipt and on a quarterly basis afterward.

Other reagents

All reagents used were obtained from commercial suppliers at research-grade or higher, unless otherwise indicated. Sulfo-SPDB-DM4 was purchased from Levena Biopharma.

Synthesis of conjugatable eribulin and cryptophycin linker payloads

Synthetic methods for conjugatable eribulin and cryptophycin compounds are provided in Supplementary Fig. S1. A

complete list of conjugatable eribulin structures for compounds utilized in this report is shown in Fig. 1.

Cysteine-based conjugation using maleimides

Antibody was buffer-exchanged into Dulbecco's PBS (DPBS), and then concentrated to 20 mg/mL using centrifugal concentration. An equal volume of 270 μmol/L tris(2-carboxyethyl)phosphine (TCEP) in 1× DPBS with 2 mmol/L EDTA was added and reduction was carried out by gentle mixing for 40–80 minutes at room temperature (reduction time was optimized for each antibody to achieve a target DAR = 4). Maleimido-linker-eribulin compound (in DMSO) was conjugated to partially reduced antibody at a molar ratio of 1:6 (antibody:compound). Compound was added to 50% propylene glycol in DPBS and mixed well, and then an equal volume of partially reduced antibody was added and mixed gently (final propylene glycol concentration of 25%). Conjugation proceeded for 3.5 to 4 hours at room temperature.

Two-step amine-based conjugation using strain-promoted alkyne–azide chemistry (SPAAC)

Antibody (farletuzumab or amatuximab, nonreduced) was brought to 10.0 mg/mL in 0.1 mol/L sodium bicarbonate, pH 8.3. Propylene glycol (50%) was prepared in 0.1 mol/L sodium bicarbonate, pH 8.3. N-hydroxysuccinimide-dibenzylcyclooctyne (NHS-DBCO; Click Chemistry Tools, 50 mmol/L in DMSO) was added to the 50% propylene glycol and mixed thoroughly, then equal volume of antibody was added at a molar ratio of 1:4 (antibody:DBCO) and mixed thoroughly. Conjugation proceeded for 1 hour at room temperature. Unreacted NHS-DBCO was removed by chromatography on G-25 resin as described below. DAR of the antibody–DBCO species was determined by absorbance spectroscopy at 309 nm. SPAAC-based conjugations using azido-linker-eribulin compounds were performed as for maleimide–eribulin compounds, except that conjugations were allowed to proceed overnight.

Preparation of farletuzumab ADCs using MC-Val-Cit-PAB-MMAF and MC-Val-Cit-PAB-MMAE

Linker-toxin and farletuzumab ADCs using MC-Val-Cit-PAB-MMAF and MC-Val-Cit-PAB-MMAE were prepared by PolyTherics Corp [now Abzena Inc; farletuzumab-(MC-Val-Cit-PAB-MMAF)] and Concortis Biosystems [farletuzumab- (MC-Val-Cit-PAB-MMAE)]. These ADCs were prepared and characterized for DAR and aggregation using analogous methods to those described in this report.

Purification of ADCs

Conjugated antibody was purified using HiTrap desalting column(s) (GE Healthcare) with chromatography performed on an FPLC (GE Healthcare) using 1× DPBS as running buffer, to remove linker-eribulin and propylene glycol. Final protein content was determined by BCA assay (Thermo Fisher Scientific).

Large-scale preparation of farletuzumab-[Mal-PEG_2-Val-Cit-pAB-eribulin] (MORAb-202)

Thirty milliliters of farletuzumab at 20 mg/mL (0.13 mmol/L, 3.9 μmol/L) in DPBS was mixed with 30 mL of 0.27 mmol/L TCEP solution (8.1 μmol/L) in 1× DPBS containing 2 mmol/L EDTA (DPBS/EDTA), and gently mixed at room temperature for 80 minutes. A total of 2.0 mL of Mal-PEG_2-VCP-eribulin (12 mmol/L in DMSO, 24 μmol/L) was added to 60 mL 50% propylene glycol in DPBS/EDTA, and mixed well. Farletuzumab/TCEP solution was added and mixed well. Conjugation proceeded for 4 hour at room temperature with gentle mixing. Unreacted Mal-PEG_2-VCP-eribulin was removed by G-25 chromatography on an AKTA FPLC using 1× DPBS as mobile phase (0.57 L column volume). Five individual runs were pooled following analytic analyses and concentrated to 10 mg/mL using tangential flow filtration (TFF). Final yield of ADC was 2.0 g (67%).

Conjugation of farletuzumab with sulfo-SPDB-DM4

Farletuzumab was buffer exchanged to 0.1 mol/L sodium bicarbonate buffer using HiTrap desalting column chromatography using an AKTA FPLC (GE Healthcare). Antibody was adjusted to 5 mg/mL in 25% propylene glycol/0.1 mol/L sodium bicarbonate buffer at pH 8.3, then conjugated with sulfo-SPDB-DM4 (Lenvena Biopharma) at molar ratio 1:25 (antibody: payload) at room temperature for 1 hour with gentle mixing. Unreacted sulfo-SPDB-DM4 was inactivated by an addition of 1:100 vol:vol of 1 mol/L Tris-HCl, pH 8.0 and further incubation for 10 minutes. Farletuzumab-sulfo SPDB-DM4 was purified by desalting chromatography on a HiTrap desalting column. DAR was determined using liquid chromatography/mass spectrometry (LC/MS).

DAR analysis by hydrophobic interaction chromatography

DAR was analyzed using hydrophobic interaction chromatography (HIC-HPLC). Samples were injected onto a TSKgel Butyl-NP5, 4.6 mm ID × 3.5 cm, 2.5 μmol/L nonporous size (Tosoh Bioscience), and eluted from the column with a 3-minute equilibration in 100% of mobile phase A, a 15-minute gradient (0–100% B), a 5-minute hold in 100% B, a 1-minute change to 100% A, and a 5-minute reequilibration in 100% of mobile phase A, at 0.7 mL/minute. Mobile phase A was 25 mmol/L sodium phosphate, 1.5 mol/L ammonium sulfate, pH 7.0. Mobile phase B was 25 mmol/L sodium phosphate, 25% isopropanol, pH 7.0. Detection was done at 280 nm (reference 320 nm). DAR was determined by the formula:

$$[AUC_{+1} + 2(AUC_{+2}) + 3(AUC_{+3}) + \ldots n(AUC_{+n})]/\Sigma AUC_{tot}]$$

where AUC_{+1} is the area under the curve for the mAb peak corresponding to ADC conjugated with one cytotoxin, AUC_{+2} is the area under the curve for the mAb peak corresponding to ADC conjugated with two cytotoxins, etc. ΣAUC_{tot} is the combined area under the curve for all peaks.

DAR analysis by LC/MS

Samples were prepared and separated by LC/MS using methods described previously (31). Data were analyzed and deconvoluted offline using MassLynx and MaxEnt1. DAR was calculated using the formula:

$$2[[AUC_{LC+1} + 2(AUC_{LC+2}) + 3(AUC_{LC+3}) + \ldots n(AUC_{LC+n})]/\Sigma I_{LC}tot] + 2[[AUC_{HC+1} + 2(AUC_{HC+2}) + 3(AUC_{HC+3}) + \ldots n(AUC_{HC+n})]/\Sigma AUC_{HC}tot]$$

where AUC_{LC+1} is area under the curve of the light-chain peak conjugated with one cytotoxin, AUC_{LC+2} is area under the curve of the light-chain peak conjugated with two cytotoxins, etc.

AUC_{HC} are the area under the curve of the corresponding heavy chains, and ΣAUC_{LC}tot and ΣAUC_{HC}tot are the combined area under the curve of all unconjugated and conjugated light chains and heavy chains, respectively.

Aggregation analysis by size-exclusion chromatography

Aggregation was analyzed by size-exclusion (SEC), HPLC (SEC-HPLC) using an Agilent 1260 HPLC (Agilent Technologies). ADC was diluted to 1 mg/mL in DPBS. The ADC (10 μL) was injected onto an Advanced SEC 300A guard column (4.6 mm × 3.5 cm, 2.7-μm pore size, Agilent), followed by a AdvancedBio 300 Å column (4.6 mm × 30 cm, 2.7-μm pore size), eluted from the column with 0.1 mol/L sodium phosphate containing 0.15 mol/L NaCl and 5% isopropanol, at pH 7.4, at a flow rate of 0.25 mL/minute for 28 minutes. All data were analyzed using Agilent ChemStation software. Percent aggregation was calculated as $[PA_{aggregate}/PA_{total}]\times 100$, where PA = integrated peak area.

Binding by surface plasmon resonance

Antibody concentrations were adjusted to 2 μg/mL in HBS-P+ buffer (GE Healthcare). Unmodified antibodies or ADCs were injected over an antihuman IgG sensor on a BIAcore T100 (GE Healthcare) for 1 minute at a flow rate of 10 μL/minute. A series of increasing concentrations of recombinant FRA was injected for 300 seconds at a flow rate of 30 μL/minute. Dissociation of antigen was monitored for 30 minutes. The sensor surface was regenerated by injecting 3 mol/L $MgCl_2$ for 2 × 30 seconds at a flow rate of 30 μL/minute. Sensograms were analyzed with Biacore T100 Evaluation Software using a 1:1 Langmuir binding model.

Endotoxin testing

Endotoxin levels were determined using the Pyrogene Recombinant Factor C Endotoxin Detection Kit (Lonza Inc), in accordance with manufacturer's instructions. Data fitting was performed using SoftMax Pro software with a linear fitting model.

Free thiol content analysis

Free thiol content was analyzed using a fluorometric thiol assay kit (Sigma), in accordance with manufacturer's instructions. Data fitting was performed using SoftMax Pro software with a linear fitting model.

ELISA

Recombinant antigen human folate receptor alpha 115 ng/mL (recombinant human FRA) or 1 μg/mL (recombinant human MSLN) in coating buffer (50 mmol/L carbonate–bicarbonate buffer, pH 9.6) were coated onto a 96-well Maxisorp black plate (Thermo Fisher Scientific; 100 μL/well) at 4°C, overnight. Coating solution was discarded and plate was washed three times using 1× PBS buffer with 0.05% Tween-20 (PBST) buffer. Plates were blocked in 300-μL blocking buffer (1% BSA in PBST) at room temperature for 2 hours on an orbital shaker. Antibodies and ADCs were diluted to 1,000 ng/mL in blocking buffer, serially diluted, and added to the plate. Plates were incubated at room temperature for 2 hours on an orbital shaker. Antibody solution was discarded and plates were washed three times as above. One-hundred microliters per well of goat-anti-human IgG(H+L)-HRP (1:10,000 dilution in blocking buffer) solution was added to the plates and plates were incubated at room temperature for 1 hour with shaking. Secondary antibody solution was discarded and plates were washed three times. One-hundred microliters per well of QuantaBlu fluorogenic peroxidase substrate working solution (Thermo Fisher Scientific) was added to the plates and plates were incubated at room temperature for 30 minutes. Fluorescence was read at excitation 325 nm/emission 420 nm using a SpectraMax M5 (Molecular Devices). Data was analyzed using SoftMaxPro 5.4.2 software with 4-parameter fitting.

Flow cytometry

Cells were harvested when approximately 80%–90% confluent using 0.25% Trypsin-EDTA solution (Thermo Fisher Scientific), washed once in PBS/1% FBS (FACS buffer), and then resuspended at 5×10^5 cells/mL. Antibody at 0.1 mg/mL was added (10 μg/mL final), and the plate was incubated on ice for 1 hour. Cells were washed three times with FACS buffer and resuspended in 100 μL of Alexa Fluor 488 goat anti-human IgG secondary antibody conjugate (Thermo Scientific). The plate was incubated on ice for 1 hour and washed three times. Cells were resuspended in 200 μL and analyzed immediately on a Guava EasyCyte 8HT flow cytometer (Millipore-Sigma Corporation). Data were analyzed using FCSExpress software.

Cytotoxic activity analysis

Cytotoxicity assays were performed as described previously (32). For competition experiments, titrated ADC was preincubated with 2 μmol/L (final) unconjugated antibody prior to incubation with cells.

In vitro matrix stability

Stability samples were prepared in pooled plasma and serum from mouse and human (Bioreclamation) in duplicate. MORAb-202 was diluted to 0.5 mg/mL in pooled matrix and divided into aliquots. The T0 sample was then frozen at −80°C. The remaining sample vials were incubated in a 37°C chamber for intervals of 24, 48, 72, 96, or 240 hours. A sample was removed at each target incubation time and transferred to −80°C until all sample timepoints were reached. Analysis was performed using a label-free bio-layer interferometry assay. Briefly, matrix samples were diluted to 1:100 in 1× PBS containing 0.05% Tween-20 and 1% BSA (assay buffer). As controls, MORAb-202, as well as DAR2 and DAR4 isolates of MORAb-202 (purified by preparative HIC chromatography), were diluted to 0.5 mg/mL in matrix and prepared as above. Biotinylated anti-farletuzumab $F(ab)_2$ AbD14628 (Bio-Rad) at 5 μg/mL in assay buffer was captured on SA streptavidin biosensor tips (300 seconds; Pall-ForteBio), followed by capture of diluted stability samples and controls (300 seconds). Payload was then quantitated by binding of rabbit-human chimeric anti-eribulin antibody 5E4 at 100 μg/mL (Supplementary Fig. S2A). This concentration was determined empirically and represents maximal binding in a DAR-dependent manner (Supplementary Fig. S2B). Association was monitored for 300 seconds, at which point binding had reached equilibrium. Binding level (R_{eq}) at end of dissociation phase was determined for each sample. Data was plotted as percent R_{eq} relative to t_0, where percent $R_{eq} = R_{eq}t_x/R_{eq}t_0(100)$.

In vivo efficacy

For NCI-H2110 xenograft model, human non–small cell lung carcinoma NCI-H2110 cells (1×10^7 cells) mixed with

matrigel at 1:1 (vol:vol) were implanted subcutaneously in female 6 weeks old CB17 SCID mice (Taconic). Tumor volume (mm^3) was measured and calculated using the formula $(W \times L \times D) \times \pi/6$. Mice were randomized when average tumor volume was approximately 150 mm^3. Mice were subsequently treated with single dose of MORAb-202 at 1, 2.5, or 5 mg/kg or with PBS (vehicle control). For pharmacokinetic assays, blood collection was performed on the day before treatment and days 1, 2, 8, 15, and 28 posttreatment. Concentrations of total antibody and intact MORAb-202 in serum were measured using DAR-insensitive MORAb-202 total antibody and intact ADC assays. LXFA-737 human NSCLC patient-derived xenograft (PDX) study was performed by Oncotest GmbH. Female NMRI nu/nu mice (NMRI-*Foxn1*^{nu}) were implanted with 3–4 mm length LXFA-737 tumor fragments from donor mice subcutaneously. Mice were randomized as above and treated with single dose of MORAb-202 at 5 mg/kg, a single dose of farletuzumab at 5 mg/kg, or with PBS. GA0055 human gastric PDX study was performed at Crown Bioscience Inc. GA0055 tumor fragments (2–3 mm) were implanted subcutaneously in 4- to 6-week-old BALB/C nude mice. Mice were randomized as above and treated with single dose of MORAb-202 at 5 mg/kg or with PBS.

IHC

FRA expression was evaluated by IHC staining using anti-FRA mAb clone 26B3 (33). Each FFPE slide was incubated with anti-FRA mAb (1 μg/mL, clone 26B3) or control murine IgG (Jackson ImmunoResearch), and bound antibody was visualized by Ultravision Quanto Mouse on Mouse Staining Kit (Thermo Fisher Scientific).

Results

Preparation and analyses of eribulin-based ADCs

A strategy was employed to evaluate the potential of eribulin as a payload for ADCs, focusing on linker addition to the primary amine group at carbon-35. This comprised analysis of both amine- (via SPAAC) and sulfhydryl-reactive antibody conjugation chemistry, various spacer lengths, and different payload release approaches. The analysis also included both cleavable and non-cleavable linker species. A schematic illustrating this approach is shown in Fig. 1.

Antibodies were prepared for cysteine conjugation by partial reduction of interchain disulfide bonds using the non-thiol reducing reagent TCEP immediately prior to reaction with maleimide–linker–eribulin compounds, or for SPAAC conjugation by attachment of DBCO to lysine residues using NHS-DBCO. In addition to farletuzumab, amatuximab, a chimerized anti-human MSLN mAb that is currently under clinical investigation for the treatment of mesothelioma (34), was also conjugated with the identical set of linker-eribulin compounds to be used as a control ADC. In each case, a DAR of 4 was targeted. Following purification of the ADCs to remove unreacted compound, ADCs were analyzed for aggregate levels by SEC-HPLC and DAR by either reverse-phase LC/MS (amine-based ADCs) or HIC-HPLC (cysteine-based ADCs). Antigen-binding studies were performed using antigen-specific ELISAs. A detailed summary of these analytic analyses is listed in Supplementary Fig. S3.

Farletuzumab and amatuximab demonstrated similar DAR and aggregate results with a given linker-eribulin species, suggesting that there were no major antibody-dependent conjugation differences. Farletuzumab ADCs had slightly higher

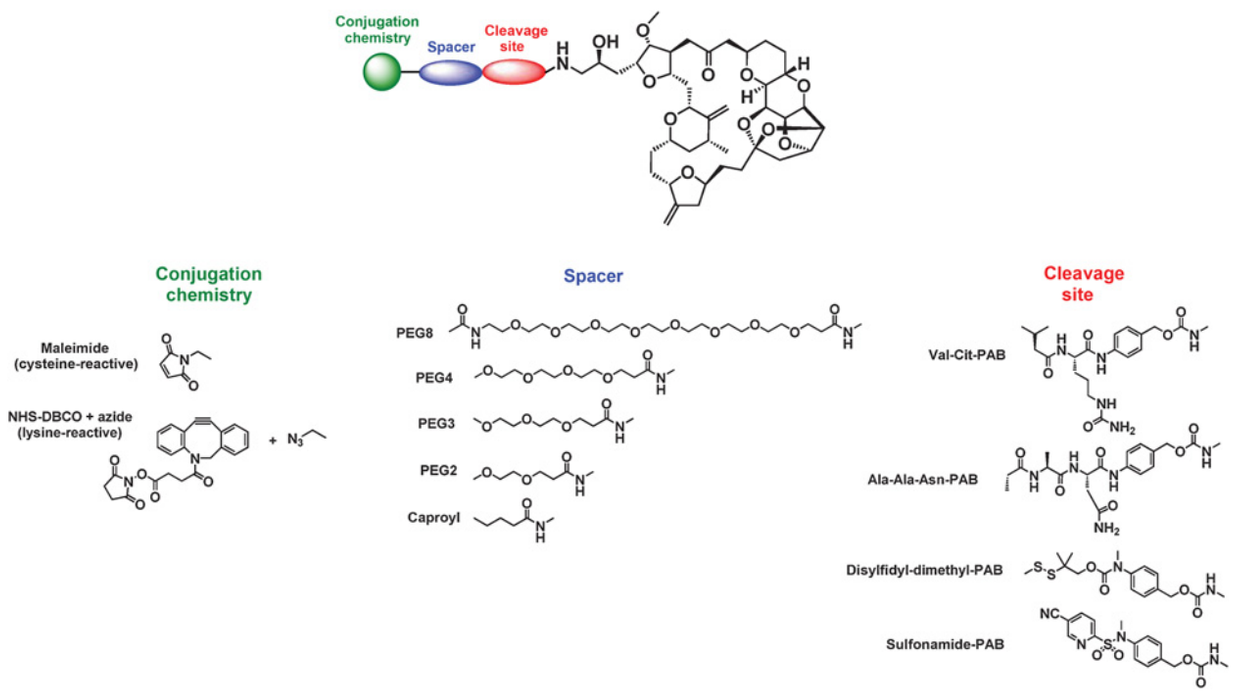

Figure 1.
Strategy for synthesis of conjugatable eribulin molecules. Structures and synthetic methods for compounds can be found in Supplementary Fig. S1.

aggregate levels than amatuximab ADCs, but this is likely attributable to the higher starting aggregate levels in the parental antibody. When caproyl or short (PEG_2) spacers were used, conjugation was efficient, with DAR in the range of 3.3 to 4.8 for maleimides and 2.8 to 3.1 for SPAAC conjugations. This was generally independent of cleavage site chemistry, although the disulfidyl-dimethyl and sulfonamide cleavage sites did demonstrate slightly lower overall DAR with PEG_3 spacers using SPAAC. Aggregate levels were also generally low (<5%), even with the more hydrophobic caproyl spacer or with inclusion of DBCO in the conjugation strategy. When the spacer was lengthened to PEG_8 (maleimide paired with a Val-Cit-PAB cleavage site) or PEG_4-triazole-PEG_3 (maleimide paired with sulfonamide or disulfide cleavage sites), aggregate levels increased significantly (5%–18%) and conjugation efficiency was negatively affected, with DAR between 0.5 and 2.3. This suggests that spacing between the conjugation site and cleavage site/eribulin payload is critical to obtaining preferred biophysical characteristics of eribulin ADCs, consistent with previous findings (35). With regard to antigen-specific binding, noncleavable maleimide-based farletuzumab ADCs were impacted the least in this screening, relative to unmodified antibody, with no significant changes observed. For other maleimide-based linker-eribulin farletuzumab ADCs, a 2- to 3-fold loss in target binding was typically observed. For amatuximab ADCs, all ADCs had less than a 2-fold drop in antigen-specific binding, relative to parental antibody. Overall, the high conjugation efficiency, low aggregate levels, and retention of antigen-specific binding achieved support the use of eribulin as an ADC payload.

In vitro potency and specificity of eribulin ADCs

ADCs were evaluated for specificity and potency in cell-based cytotoxicity assays. The cell lines chosen were IGROV1, which expresses high levels of FRA (FRA^{hi}, farletuzumab-reactive; ref. 30), but no MSLN, NCI-H2110, which expresses moderate levels of both FRA and MSLN (FRA^{mod}/$MSLN^{mod}$, farletuzumab- and amatuximab-reactive), and A431, which is negative for expression of both antigens. A subset of cytotoxicity data, with farletuzumab as conjugated antibody, is shown in Table 1. A complete dataset is listed in Supplementary Fig. S3.

Overall, potency on the FRA^{hi} cell line IGROV1 was robust for all farletuzumab ADCs, in the 10^{-10}–10^{-9} mol/L range, with specificity ratios of 2–3 logs compared with the analogous amatuximab ADCs. On the FRA^{mod}/$MSLN^{mod}$ cell line NCI-H2110, potency of the farletuzumab ADCs was generally lower, which was expected on the basis of the lower surface antigen expression compared with IGROV1. Interestingly, the MSLN-binding amatuximab ADCs were all lower in potency than their farletuzumab equivalents, even with similar DARs. Becausee the binding affinity of amatuximab is greater than farletuzumab to its respective antigen (0.1 nmol/L vs. 12 nmol/L) and the expression levels of FRA and MSLN in these cells are comparable, these data suggest that FRA internalization and processing/turnover better mediates ADC-elicited cytotoxicity. Comparable results were observed for both maleimide- and SPAAC-based conjugation chemistry using either PEG_x-Val-Cit-PAB or $PEG_{2/4}$ noncleavable linkers (the slightly lower potency for the SPAAC noncleavable constructs is likely due to the slightly lower DAR in these species). This suggests that there is no preferable modality of conjugation for eribulin ADCs, in terms of potency and specificity. When the length of the PEG spacer group was varied, potency results were also similar, irrespective of the spacer length. This observation was consistent for both noncleavable and Val-Cit–containing linkers.

Significant differences were observed among farletuzumab ADCs generated by using linkers with different cleavage chemistry. Both Val-Cit-PAB and Ala-Ala-Asn-PAB–containing linkers demonstrated robust potency and specificity on IGROV1 cells, but Val-Cit-PAB ADCs retained better specificity on the FRA^{med} cell line NCI-H2110 (5-fold) compared with Ala-Ala-Asn-PAB (<2-fold). In addition, Ala-Ala-Asn-PAB linkers showed low, but significant, cytotoxicity on the negative cell line A431. ADCs with disulfidyl-dimethyl–containing linkers and sulfonamide-containing linkers were only specific on IGROV1 cells, and had high levels of off-target killing on A431 cells for both cysteine and lysine conjugation strategies. ADCs with noncleavable linkers demonstrated excellent specificity on IGROV1 cells, albeit potency tended to be lower than with other linkers. In contrast, these noncleavable farletuzumab ADCs demonstrated very weak and nonspecific cytotoxicity on NCI-H2110 cells, indicating that, with lower cell

Table 1. Analyses of farletuzumab ADCs

				Cytotoxicity analysis (IC_{50}, nmol/L)			
Payload	**Conjugation chemistry**	**Spacer**	**Cleavage chemistry**	**IGROV1**	**NCI-H2110**	**A431**	**SJSA1**
Eribulin	Maleimide	PEG2	Val-cit-pAB	0.10	3.7	>100	>100
Eribulin	Maleimide	PEG8	Val-cit-pAB	0.12	7.1	86	n.t.
Eribulin	Maleimide	Caproyl	Val-cit-pAB	0.11	3.9	>100	n.t.
Eribulin	Maleimide	PEG2	Ala-ala-asn-pAB	0.080	3.8	32	n.t.
Eribulin	Maleimide	PEG4-triazole-PEG3	Disulfidyl-dimethyl-pAB	0.27	0.85	7.0	n.t.
Eribulin	Maleimide	PEG4-triazole-PEG3	Sulfonamide	0.37	0.69	6.8	n.t.
Eribulin	Maleimide	PEG2	None	0.33	38	>100	n.t.
Eribulin	Maleimide	PEG4	None	0.28	22	>100	n.t.
Eribulin	Succinamide/SPAAC	PEG4	Val-cit-pAB	0.038	4.3	>100	n.t.
Eribulin	Succinamide/SPAAC	PEG3	Disylfidyl-dimethyl-pAB	0.55	0.90	9.7	n.t.
Eribulin	Succinamide/SPAAC	PEG3	Sulfonamide	1.8	1.7	25	n.t.
Eribulin	Succinamide/SPAAC	PEG2	None	4.3	38	>100	n.t.
Eribulin	Succinamide/SPAAC	PEG4	None	1.3	46	>100	n.t.
Cryptophycin	Maleimide	PEG2	Val-cit-pAB	0.030	n.t.	n.t.	>100
MMAE	Maleimide	Caproyl	Val-cit-pAB	0.20	n.t.	n.t.	>100
MMAF	Maleimide	Caproyl	Val-cit-pAB	1.0	n.t.	n.t.	>100
Eribulin	n/a	n/a	n/a	0.32	0.20	0.65	2.9

NOTE: IC_{50} values represent averages of at least two independent assays.
Abbreviations: n/a, not applicable; n.t., not tested.

Table 2. *In vitro* cytotoxicity of MORAb-202 and eribulin on various FRA-positive cell lines

Cell line	Cell line origin	FRA Expression	IC_{50}	
			MORAb-202	Eribulin IC_{50}
IGROV1	Ovarian	+++	0.02 ± 0.00	0.28 ± 0.17
OVCAR-3	Ovarian	++	0.75 ± 0.36	0.10 ± 0.03
CaOV3	Ovarian	++	4.26 ± 0.53	0.44 ± 0.00
NCI-H2110	NSCLC	++	0.42 ± 0.11	0.19 ± 0.01
MKN7	Gastric	++	2.17 ± 0.91	0.18 ± 0.01
MKN74	Gastric	++	1.76 ± 0.88	0.21 ± 0.02
NCI-N87	Gastric	+	4.42 ± 0.11	0.21 ± 0.01
NUGC3	Gastric	±	24.58 ± 4.41	0.14 ± 0.01
HEC-251	Endometrial	++	13.15 ± 2.32	0.36 ± 0.03
HEC-1-A	Endometrial	++	1.81 ± 0.21	0.24 ± 0.04
HEC-59	Endometrial	+	1.03 ± 0.54	0.06 ± 0.02
HCC1954	TNBC	+	1.42 ± 0.31	0.25 ± 0.01
A431	Epidermoid	−	>100	0.78 ± 0.03

NOTE: Values are averages of at least three independent assays. +++, mean fluorescence intensity (MFI) > 500; ++, MFI 50–500; +, MFI 20–50; ± MFI 5–20; −, MFI < 5.

surface expression, cleavage and release of the parental eribulin payload is required.

Comparison of Mal-PEG_2-Val-Cit-PAB-eribulin with other MTA payloads

Farletuzumab was also conjugated to a number of other Val-Cit-PAB–linked-MTA payloads to compare with farletuzumab-[Mal-PEG_2-Val-Cit-PAB-eribulin]. DAR and aggregation were evaluated as well as potency and specificity on IGROV1 (FRA^{hi}) and SJSA1 (FRA^{neg}) cell lines. These results are shown in Table 1. Farletuzumab-[Mal-PEG_2-Val-Cit-PAB-eribulin] demonstrated higher potency on IGROV1 cells than other farletuzumab ADCs, with the exception of farletuzumab-[Mal-PEG_2-Val-Cit-PAB-cryptophycin]. However, farletuzumab-[Mal-PEG_2-Val-Cit-PAB-cryptophycin] ADC demonstrated unacceptably high levels of aggregate formation under the conjugation conditions employed in this study.

Generation of MORAb-202

The biophysical and cytotoxicity screening results from the various eribulin-linker farletuzumab ADC constructs lead to the conclusion that farletuzumab-[Mal-PEG_2-Val-Cit-PAB-eribulin] was the preferred ADC format among all those tested. The preparation of this ADC, hereafter referred to as MORAb-202, was scaled up to gram-level and replicate conjugations were performed to investigate the reproducibility and robustness of the process, along with a more extensive analytic analysis of the replicate runs and final material (Supplementary Fig. S4). MORAb-202 conjugations were highly consistent between preparations, demonstrating reproducibility of the conjugation process. Aggregation levels were very low (1.3%) at an ADC concentration of 10 mg/mL, even utilizing a simple PBS formulation with no added nonionic detergents. Free thiol content was also low (1.0 %), demonstrating high conjugation efficiency and occupancy of the reduced disulfides.

In vitro potency and specificity of MORAb-202–mediated cytotoxicity against various FRA-positive cell lines

MORAb-202 potency was evaluated on a number of tumor cell lines varying in anatomical origin and FRA expression. The results of this analysis are shown in Table 2. As it was observed during the screening of other eribulin-based ADCs, MORAb-202 was highly potent (20 pmol/L IC_{50}) on the FRA^{hi} tumor cell line IGROV1. Subnanomolar potency was also observed on NCI-H2110 and OVCAR-3 cells, with nanomolar potency on cell lines of moderate to low expression of FRA across multiple tumor cell line origins. These results suggested that MORAb-202 may be useful in targeting FRA-expressing tumors regardless of tissue origin or FRA cell surface expression levels. Antigen specificity of MORAb-202 cytotoxicity was investigated using a competition assay format (Supplementary Fig. S5). Coincubation with unconjugated farletuzumab resulted in a 2-log shift in potency on IGROV1 cells, demonstrating the cytotoxic effects of MORAb-202 are antigen-driven.

Mal-Val-Cit-PAB-eribulin payload comparison with sulfo-SPDB-DM4 conjugated to farletuzumab

Previous work using an anti-FRA ADC utilizing the protected disulfide-linked microtubule-targeting agent maytansine linker payload sulfo-SPDB-DM4 has been reported to be effective against FRA-positive tumor cells (36). To compare the utility of the Mal-PEG_2-Val-Cit-PAB-eribulin with sulfo-SPDB-DM4 as an ADC linker-payload targeting FRA, sulfo-SPDB-DM4 was conjugated to farletuzumab at a DAR of 3.5, similar to previously reported (37), and evaluated for potency and specificity. These results are shown in Table 3. Free eribulin demonstrated equivalent or higher potency than DM4 on all cell lines evaluated.

Table 3. *In vitro* potency comparison of MORAb-202 with farletuzumab conjugated with sulfo-SPDB-DM4

Cell line	FRA Expression	IC_{50} (nmol/L)			
		MORAb-202	Farletuzumab-sulfo SPDB-DM4	Eribulin	DM4
IGROV1	+++	0.01 ± 0.00	0.09 ± 0.00	0.89 ± 0.04	2.56 ± 0.04
OVCAR3-A1	+++	0.06 ± 0.01	0.49 ± 0.01	0.15 ± 0.00	0.19 ± 0.01
NCI-H2110	++	2.20 ± 0.20	0.52 ± 0.01	0.27 ± 0.02	0.44 ± 0.01
NCI-N87	+	3.64 ± 0.47	0.82 ± 0.09	0.17 ± 0.02	0.69 ± 0.02
A431	−	>100	4.27 ± 0.86	1.05 ± 0.00	1.72 ± 0.06

NOTE: DAR of farletuzumab-sulfo-SPDB-DM4 was 3.5 (data not shown). IC_{50} values represent an average of three independent assays.

MORAb-202 was 8- to 9-fold more potent on FRA^{hi} cell lines than farletuzumab-[sulfo-SPDB-DM4]$_{3.5}$, while having 1.9- to 4.8-fold lower potency on FRA^{mod}/FRA^{low} cell lines. Importantly, MORAb-202 demonstrated higher specificity (27- to >1,000-fold vs. FRA^{neg} cell line A431) under these assay conditions. In contrast, farletuzumab-[sulfo-SPDB-DM4]$_{3.5}$ specificity was significantly lower (5.2- to 47-fold vs. FRA^{neg} cell line A431).

In vivo efficacy of MORAb-202

MORAb-202 was evaluated for *in vivo* efficacy in an NCI-H2110 xenograft model in CB17 SCID mice. This model was selected on the basis of the reproducible and robust growth of NCI-H2110 tumors in SCID mice, its demonstrated sensitivity to free eribulin treatment (0.2 mg/kg MED q4d×3, Supplementary Fig. S6), along with its moderate levels of FRA expression to allow for a more conservative evaluation. *In vitro* stability of MORAb-202 in mouse and human plasma and serum using a DAR-sensitive label-free binding assay suggested that linker-payload plasma stability of [Mal-PEG_2-Val-Cit-PAB-eribulin] was consistent with previous studies using Val-Cit–containing linker-payloads conjugated to reduced disulfides via maleimides, in that a measureable amount of payload release is detectable; however, the majority of ADC remains intact (Fig. 2A and B; refs. 38, 39). On the basis of assay performance using individual DAR species, MORAb-202 was at a DAR of approximately 3 after 240-hour incubation in either human or mouse plasma or serum.

MORAb-202 was administered as a single dose intravenously at 1 mg/kg, 2.5 mg/kg, and 5 mg/kg, to evaluate dose-dependent effects. The results of this study are shown in Fig. 3A. At 1 mg/kg, MORAb-202 had a marginal effect on tumor growth in this model. At the 2.5 mg/kg dose, it induced prolonged tumor growth inhibition; however, this dose level did not prevent tumors from eventually regrowing. MORAb-202 at 5 mg/kg induced a complete response, as all mice were tumor-free at end of study. At the 5 mg/kg dose, there was no effect on body weight in treated animals. Pharmacokinetics of MORAb-202 in NCI-H2110–bearing mice indicated the majority (> 50%) of MORAb-202 remains intact 8–15 days postadministration (Fig. 2C).

MORAb-202 was also evaluated for efficacy in PDX models of NSCLC and gastric cancer, which have both been shown to overexpress FRA (24, 40). As with the NCI-H2110 model, these models were selected on the basis of moderate FRA expression and their reproducible, robust growth in immunocompromised mice. In both models, MORAb-202 was administered as a single dose intravenously at 5 mg/kg. Results from these studies are shown in Fig 3B and C. Consistent with results from the NCI-H2110 study, durable tumor growth inhibition was observed in both PDX models, with a complete response in 4 of 6 mice for the lung LXFA-737 model and 1 of 6 mice for the gastric GA0055 model. In the LXFA-737 model, farletuzumab at an equal dose to MORAb-202 had no effect on tumor growth. Regrown tumors from this study were also analyzed for FRA expression and remained FRA-positive, suggesting that these tumors would be sensitive to retreatment with MORAb-202 (Supplementary Fig. S7A and S7B, isotype control and MORAb-202–treated, respectively).

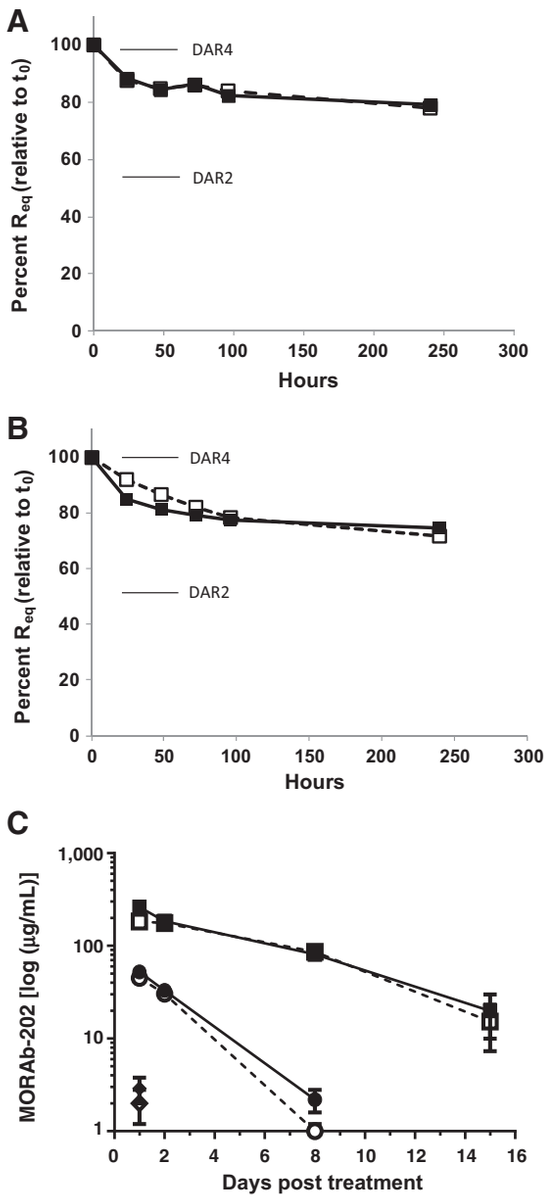

Figure 2.

In vitro matrix stability and *in vivo* pharmacokinetics in NCI-H2110 tumor-bearing mice of MORAb-202. **A,** Stability of MORAb-202 in mouse and human plasma *in vitro* at 37°C. Data are plotted as percentage of equilibrium binding (R_{eq}) of anti-eribulin antibody 5E4 at t_0 and is normalized for matrix-only. Groups are as follows: ---□---, mouse plasma; ——■——, human plasma. Indicated on the chart are equilibrium binding values (as percentage of t_0) of purified DAR2 and DAR4 species of MORAb-202 freshly diluted in matrix, for reference (DAR0 MORAb-202 demonstrated no 5E4 binding). **B,** Stability of MORAb-202 in mouse and human serum *in vitro* at 37°C. Data were plotted similarly as in **A**. Groups are as follows: ---□---, mouse serum; ——■——, human serum. **C,** Pharmacokinetics of MORAb-202 in NCI-H2110 tumor-bearing mice. Groups are as follows, open data markers with dashed lines, intact MORAb-202; closed data markers with solid lines, total antibody. Dose levels were 1 mg/kg, 5 mg/kg, and 25 mg/kg.

Discussion

Targeting the tubulin polymerization/depolymerization mechanism using highly potent MTAs as payloads for ADCs is an intensive area of research that has been ongoing for many years.

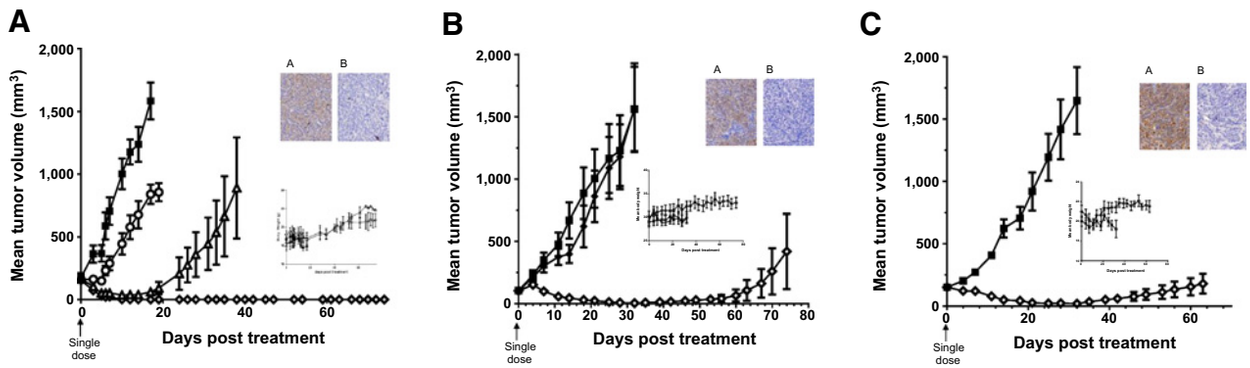

Figure 3.

In vivo efficacy of MORAb-202. In all studies, dosing was a single dose administered intravenously. Dose groups are as follows: ■, vehicle; ○, MORAb-202, 1 mg/kg; △, MORAb-202, 2.5 mg/kg; ◇, MORAb-202, 5 mg/kg, ◆, farletuzumab, 5 mg/kg. Body weights of treated mice are shown as inset in the main graph. Tumors from untreated mice were also harvested and stained for FRA expression by IHC as detailed in Materials and Methods. These results are shown in top right of each graph: **A,** FRA-stained; **B,** IgG-control stained. **A,** NCI-H2110 human NSCLC xenograft in SCID mice, 5 mice per group (5/5 CR in 5 mg/kg MORAb-202 group). **B,** LXFA-737 NSCLC PDX in nude mice, 6 mice per group (4/6 CR). **C,** GA0055 gastric PDX in nude mice, 6 mice per group (1/6 CR).

While two of the three commercially approved ADCs have utilized MTAs as payloads, the large number of clinical trials discontinued using MTA-based ADCs suggests that improvements are needed for maximizing the potential of this class of ADCs through optimizing linker and conjugation strategies, MTA potency, and the antigen-targeting specificity of the antibody used (9). Here we describe for the first time the use of eribulin as a payload for ADCs. Eribulin represents a new type of MTA payload, in that it is highly specific for the β-subunit on the (+) termini of microtubules, potently inhibiting further extension while having little effect on depolymerization. ADCs prepared using eribulin conjugated to the FRA-targeting antibody farletuzumab demonstrated nanomolar or subnanomolar potency on FRA-positive tumor cells. Farletuzumab conjugated with Mal-PEG_2-Val-Cit-PAB-eribulin demonstrated equal or better potency *in vitro* compared with cathepsin-cleavable farletuzumab ADCs prepared with a number of other commonly investigated MTA payloads, *in vitro* stability in mouse and human matrix consistent with maleimide-conjugated Val-Cit – containing ADCs, and a complete response in *in vivo* xenograft tumor models.

The majority of ADCs currently under investigation utilize facilitated release of the payload via either chemical (low pH- or thiol reducible) or enzymatic means (9, 41). In our screening, we found that maximal potency and specificity of eribulin ADCs could be achieved when eribulin was paired with lysosomal enzyme–cleavable linkers, whereby the cathepsin-cleavable Val-Cit linkers showed better overall specificity than a legumain-cleavable Ala-Ala-Asn linker (42). Reducible dimethyl-protected disulfide-containing linkers had significant off-target cytotoxicity. Interestingly, noncleavable linkers also showed significant activity, but were only effective on cell line expressing very high levels of target antigen. Crystallographic studies on eribulin–tubulin completes demonstrated that the amine at C-35 of eribulin is exposed to solvent and that a fluorescent dye conjugate of eribulin attached at the primary amine bound tubulin with equal affinity to unmodified eribulin (13). Cysteine-linker-eribulin species, the likely metabolite of lysosomal processing of noncleavable eribulin ADCs, would thus be predicted to also be active as an MTA. We speculate that the difference is likely due to lower efficiency of lysosomal processing and metabolite release of the noncleavable ADCs, necessitating a higher cellular uptake of ADC through higher surface expression of target antigen.

A number of ADCs have been reported to utilize payloads that impart undesirable biophysical properties to the resultant conjugate, requiring limiting conjugate load via antibody engineering or postconjugation chromatographic removal of higher DAR species (43–45). ADCs with reduced hydrophobicity have been shown to lead to improved pharmacokinetics and improved therapeutic index in animal models (35, 46). Eribulin, unlike many other ADC payloads, is highly water-soluble (>10 mg/mL). Using straightforward conjugation conditions, eribulin could be conjugated to two different antibodies with DAR $\geq$ 4, with low aggregate levels achieved using nearly all of the linkers analyzed. MORAb-202, comprising farletuzumab conjugated to Mal-PEG_2-Val-Cit-PAB-eribulin at a DAR of 4.0, was reproducibly prepared with aggregate levels of 1.2%–1.3% in a neutral phosphate buffer without postconjugation targeted chromatographic removal of aggregates.

Eribulin presents a unique opportunity to investigate a compound that has a number of beneficial nonmitotic properties, in addition to its potent antimitotic properties, as an ADC payload. Eribulin has been shown to inhibit epithelial-to-mesenchymal transition (EMT), which has been associated with a more immunosuppressive tumor microenvironment (19, 20), and enhance infiltration of tumor-infiltrating lymphocytes (47). In addition, eribulin also increases vascular perfusion in tumors and reduces hypoxia. We hypothesize that the targeting of eribulin to the tumor site via conjugation to an antibody, in addition to causing direct cytotoxicity of antigen-positive tumor cells, may enhance the chemosensitivity of these cancers by transitioning them to a more susceptible epithelial phenotype and increasing the tumor penetration of coadministered chemotherapeutic regimens. Using MORAb-202, FRA-positive tumors may benefit significantly from this approach, as FRA expression has been correlated with poor prognosis in triple-negative breast cancer (TNBC; ref. 48), endometrial (49), and ovarian cancer (50, 51). MORAb-202 may offer an improvement over existing ADCs under clinical

investigation, as our preliminary comparison of Mal-PEG_2-Val-Cit-PAB-eribulin with sulfo-SPDB-DM4 conjugated to farletuzumab suggests that the eribulin linker-payload has improved specificity. Our future studies will continue to examine this payload comparison in appropriate *in vivo* models of disease.

In summary, we have demonstrated the utility of the microtubule-targeting agent eribulin as an effective payload for ADCs in *in vitro* and *in vivo* preclinical studies. Eribulin was compatible with a number of linker and conjugation formats, and ADCs exhibited both robust potency and specificity. MORAb-202, an ADC comprising the FRA-targeting antibody farletuzumab and a cathepsin-cleavable eribulin-linker payload, demonstrated the ability to elicit a potent and durable response in multiple xenograft models of disease. Recently, a phase I first-in-human, dose-escalation study to evaluate the safety and preliminary efficacy of MORAb-202 in patients with FRA-expressing solid tumors was initiated in Japan (MORAb-202-J081-101).

Disclosure of Potential Conflicts of Interest

No potential conflicts of interest were disclosed.

Disclaimer

MORAb-202 described in this article is investigational, as efficacy and safety have not been established. There is no guarantee that this ADC will be available commercially.

Authors' Contributions

Conception and design: U. Majumder, K. Furuuchi, F.G. Fang, T. Uenaka, L. Grasso, E.F. Albone

Development of methodology: X. Cheng, J. Li, K. Tanaka, U. Majumder, A.Z. Milinichik, C.J. Maddage, K.A. Rybinski, S. Fernando, D. Fernando, M. Kuc, K. Furuuchi, F.G. Fang, L. Grasso, E.F. Albone

Acquisition of data (provided animals, acquired and managed patients, provided facilities, etc.): X. Cheng, J. Li, A.Z. Milinichik, C.J. Maddage, K.A. Rybinski, M. Kuc, K. Furuuchi, F.G. Fang, E.F. Albone

Analysis and interpretation of data (e.g., statistical analysis, biostatistics, computational analysis): X. Cheng, A.Z. Milinichik, A.C. Verdi, C.J. Maddage, S. Fernando, M. Kuc, K. Furuuchi, F.G. Fang, L. Grasso, E.F. Albone

Writing, review, and/or revision of the manuscript: X. Cheng, J. Li, U. Majumder, K. Furuuchi, F.G. Fang, T. Uenaka, L. Grasso, E.F. Albone

Administrative, technical, or material support (i.e., reporting or organizing data, constructing databases): J. Li, C.J. Maddage, K. Furuuchi, E.F. Albone

Study supervision: X. Cheng, J. Li, C.J. Maddage, K. Furuuchi, T. Uenaka, L. Grasso, E.F. Albone

Other (synthesis of ADCs, drug conjugates, as well as other chemical materials to support the research, collect structural characterization data for all chemicals): J. Li

The costs of publication of this article were defrayed in part by the payment of page charges. This article must therefore be hereby marked *advertisement* in accordance with 18 U.S.C. Section 1734 solely to indicate this fact.

Received December 7, 2017; revised April 26, 2018; accepted September 20, 2018; published first September 27, 2018.

References

1. Akhmanova A, Steinmetz MO. Control of microtubule organization and dynamics: two ends in the limelight. Nat Rev Mol Cell Biol 2015;16:711–26.
2. Borisy G, Heald R, Howard J, Janke C, Musacchio A, Nogales E. Microtubules: 50 years on from the discovery of tubulin. Nat Rev Mol Cell Biol 2016;17:322–8.
3. Dumontet C, Jordan MA. Microtubule-binding agents: a dynamic field of cancer therapeutics. Nat Rev Drug Discov 2010;9:790–803.
4. Stanton RA, Gernert KM, Nettles JH, Aneja R. Drugs that target dynamic microtubules: a new molecular perspective. Med Res Rev 2011;31:443–81.
5. Vindya NG, Sharma N, Yadav M, Ethiraj KR. Tubulins - the target for anticancer therapy. Curr Top Med Chem 2015;15:73–82.
6. Issell BF, Crooke ST. Maytansine. Cancer Treat Rev 1978;5:199–207.
7. Krug LM, Miller VA, Kalemkerian GP, Kraut MJ, Ng KK, Heelan RT, et al. Phase II study of dolastatin-10 in patients with advanced non-small-cell lung cancer. Ann Oncol 2000;11:227–8.
8. Edelman MJ, Gandara DR, Hausner P, Israel V, Thornton D, DeSanto J, et al. Phase 2 study of cryptophycin 52 (LY355703) in patients previously treated with platinum based chemotherapy for advanced non-small cell lung cancer. Lung Cancer 2003;39:197–9.
9. Beck A, Goetsch L, Dumontet C, Corvaia N. Strategies and challenges for the next generation of antibody-drug conjugates. Nat Rev Drug Discov 2017;16:315–37.
10. Moskowitz CH, Nademanee A, Masszi T, Agura E, Holowiecki J, Abidi MH, et al. Brentuximab vedotin as consolidation therapy after autologous stem-cell transplantation in patients with Hodgkin's lymphoma at risk of relapse or progression (AETHERA): a randomised, double-blind, placebo-controlled, phase 3 trial. Lancet 2015;385:1853–62.
11. Verma S, Miles D, Gianni L, Krop IE, Welslau M, Baselga J, et al. Trastuzumab emtansine for HER2-positive advanced breast cancer. N Engl J Med 2012;367:1783–91.
12. Hirata Y, Uemura D. Halichondrins - antitumor polyether macrolides from a marine sponge. Pure and Applied Chemistry 1986;58:701–10.
13. Doodhi H, Prota AE, Rodriguez-Garcia R, Xiao H, Custar DW, Bargsten K, et al. Termination of protofilament elongation by eribulin induces lattice defects that promote microtubule catastrophes. Curr Biol 2016;26:1713–21.
14. Cortes J, O'Shaughnessy J, Loesch D, Blum JL, Vahdat LT, Petrakova K, et al. Eribulin monotherapy versus treatment of physician's choice in patients with metastatic breast cancer (EMBRACE): a phase 3 open-label randomised study. Lancet 2011;377:914–23.
15. Chanez B, Goncalves A, Badache A, Verdier-Pinard P. Eribulin targets a ch-TOG-dependent directed migration of cancer cells. Oncotarget 2015;6:41667–78.
16. Agoulnik SI, Kawano S, Taylor N, Oestreicher J, Matsui J, Chow J, et al. Eribulin mesylate exerts specific gene expression changes in pericytes and shortens pericyte-driven capillary network *in vitro*. Vasc Cell 2014;6:3.
17. Funahashi Y, Okamoto K, Adachi Y, Semba T, Uesugi M, Ozawa Y, et al. Eribulin mesylate reduces tumor microenvironment abnormality by vascular remodeling in preclinical human breast cancer models. Cancer Sci 2014;105:1334–42.
18. Ueda S, Saeki T, Takeuchi H, Shigekawa T, Yamane T, Kuji I, et al. *In vivo* imaging of eribulin-induced reoxygenation in advanced breast cancer patients: a comparison to bevacizumab. Br. J Cancer 2016;114:1212–8.
19. Terashima M, Sakai K, Togashi Y, Hayashi H, De Velasco MA, Tsurutani J, et al. Synergistic antitumor effects of S-1 with eribulin *in vitro* and *in vivo* for triple-negative breast cancer cell lines. SpringerPlus 2014;3:417.
20. Yoshida T, Ozawa Y, Kimura T, Sato Y, Kuznetsov G, Xu S, et al. Eribulin mesilate suppresses experimental metastasis of breast cancer cells by reversing phenotype from epithelial-mesenchymal transition (EMT) to mesenchymal-epithelial transition (MET) states. Br J Cancer 2014;110:1497–505.
21. Jain S, Vahdat LT. Eribulin mesylate. Clin Cancer Res 2011;17:6615–22.
22. Wozniak KM, Wu Y, Farah MH, Littlefield BA, Nomoto K, Slusher BS. Neuropathy-inducing effects of eribulin mesylate versus paclitaxel in mice with preexisting neuropathy. Neurotox Res 2013;24:338–44.
23. Benbow SJ, Wozniak KM, Kulesh B, Savage A, Slusher BS, Littlefield BA, et al. Microtubule-targeting agents eribulin and paclitaxel differentially affect neuronal cell bodies in chemotherapy-induced peripheral neuropathy. Neurotox Res 2017;32:151–62.
24. O'Shannessy DJ, Yu G, Smale R, Fu YS, Singhal S, Thiel RP, et al. Folate receptor alpha expression in lung cancer: diagnostic and prognostic significance. Oncotarget 2012;3:414–25.

25. O'Shannessy DJ, Somers EB, Maltzman J, Smale R, Fu YS. Folate receptor alpha (FRA) expression in breast cancer: identification of a new molecular subtype and association with triple negative disease. SpringerPlus 2012;1:22.
26. O'Shannessy DJ, Somers EB, Smale R, Fu YS. Expression of folate receptor-alpha (FRA) in gynecologic malignancies and its relationship to the tumor type. Int J Gynecol Pathol 2013;32:258–68.
27. Lin J, Spidel JL, Maddage CJ, Rybinski KA, Kennedy RP, Krauthauser CL, et al. The antitumor activity of the human FOLR1-specific monoclonal antibody, farletuzumab, in an ovarian cancer mouse model is mediated by antibody-dependent cellular cytotoxicity. Cancer Biol Ther 2013;14: 1032–8.
28. Vergote I, Armstrong D, Scambia G, Teneriello M, Sehouli J, Schweizer C, et al. A randomized, double-blind, placebo-controlled, phase III study to assess efficacy and safety of weekly farletuzumab in combination with carboplatin and taxane in patients with ovarian cancer in first platinum-sensitive relapse. J Clin Oncol 2016;34:2271–8.
29. Kline JB, Kennedy RP, Albone E, Chao Q, Fernando S, McDonough JM, et al. Tumor antigen CA125 suppresses antibody-dependent cellular cytotoxicity (ADCC) via direct antibody binding and suppressed Fc-gamma receptor engagement. Oncotarget 2017;8:52045–60.
30. Smith-Jones PM, Pandit-Taskar N, Cao W, O'Donoghue J, Philips MD, Carrasquillo J, et al. Preclinical radioimmunotargeting of folate receptor alpha using the monoclonal antibody conjugate DOTA-MORAb-003. Nucl Med Biol 2008;35:343–51.
31. Spidel JL, Vaessen B, Albone EF, Cheng X, Verdi A, Kline JB. Site-specific conjugation to native and engineered lysines in human immunoglobulins by microbial transglutaminase. Bioconjug Chem 2017;28:2471–84.
32. Albone EF, Spidel JL, Cheng X, Park YC, Jacob S, Milinichik AZ, et al. Generation of therapeutic immunoconjugates via residue-specific conjugation technology (RESPECT) utilizing a native cysteine in the light chain framework of *Oryctolagus cuniculus*. Cancer Biol Ther 2017;18:347–57.
33. O'Shannessy DJ, Somers EB, Albone E, Cheng X, Park YC, Tomkowicz BE, et al. Characterization of the human folate receptor alpha via novel antibody-based probes. Oncotarget 2011;2:1227–43.
34. Hassan R, Kindler HL, Jahan T, Bazhenova L, Reck M, Thomas A, et al. Phase II clinical trial of amatuximab, a chimeric antimesothelin antibody with pemetrexed and cisplatin in advanced unresectable pleural mesothelioma. Clin Cancer Res 2014;20:5927–36.
35. Lyon RP, Bovee TD, Doronina SO, Burke PJ, Hunter JH, Neff-LaFord HD, et al. Reducing hydrophobicity of homogeneous antibody-drug conjugates improves pharmacokinetics and therapeutic index. Nat Biotechnol 2015;33:733–5.
36. Ab O, Whiteman KR, Bartle LM, Sun X, Singh R, Tavares D, et al. IMGN853, a folate receptor-alpha (FRalpha)-targeting antibody-drug conjugate, exhibits potent targeted antitumor activity against fralpha-expressing tumors. Mol Cancer Ther 2015;14:1605–13.
37. Moore KN, Borghaei H, O'Malley DM, Jeong W, Seward SM, Bauer TM, et al. Phase 1 dose-escalation study of mirvetuximab soravtansine (IMGN853), a folate receptor alpha-targeting antibody-drug conjugate, in patients with solid tumors. Cancer 2017;123:3080–7.
38. Doronina SO, Toki BE, Torgov MY, Mendelsohn BA, Cerveny CG, Chace DF, et al. Development of potent monoclonal antibody auristatin conjugates for cancer therapy. Nat Biotechnol 2003;21:778–84.
39. Lyon RP, Setter JR, Bovee TD, Doronina SO, Hunter JH, erson ME, et al. Self-hydrolyzing maleimides improve the stability and pharmacological properties of antibody-drug conjugates. Nat Biotechnol 2014;32:1059–62.
40. Assaraf YG, Leamon CP, Reddy JA. The folate receptor as a rational therapeutic target for personalized cancer treatment. Drug Resist Updat 2014;17:89–95.
41. Chen H, Lin Z, Arnst KE, Miller DD, Li W. Tubulin inhibitor-based antibody-drug conjugates for cancer therapy. Molecules 2017;22:1–26.
42. Bajjuri KM, Liu Y, Liu C, Sinha SC. The legumain protease-activated auristatin prodrugs suppress tumor growth and metastasis without toxicity. ChemMedChem 2011;6:54–9.
43. Hamblett KJ, Senter PD, Chace DF, Sun MM, Lenox J, Cerveny CG, et al. Effects of drug loading on the antitumor activity of a monoclonal antibody drug conjugate. Clin Cancer Res 2004;10:7063–70.
44. Elgersma RC, Coumans RG, Huijbregts T, Menge WM, Joosten JA, Spijker HJ, et al. Design, synthesis, and evaluation of linker-duocarmycin payloads: toward selection of HER2-targeting antibody-drug conjugate SYD985. Mol Pharm 2015;12:1813–35.
45. Strop P, Delaria K, Foletti D, Witt JM, Hasa-Moreno A, Poulsen K, et al. Site-specific conjugation improves therapeutic index of antibody drug conjugates with high drug loading. Nat Biotechnol 2015;33:694–6.
46. Panowski S, Bhakta S, Raab H, Polakis P, Junutula JR. Site-specific antibody drug conjugates for cancer therapy. MAbs 2014;6:34–45.
47. Kashiwagi S, Asano Y, Goto W, Takada K, Takahashi K, Noda S, et al. Use of Tumor-infiltrating lymphocytes (TILs) to predict the treatment response to eribulin chemotherapy in breast cancer. PLoS One 2017;12:e0170634.
48. Zhang Z, Wang J, Tacha DE, Li P, Bremer RE, Chen H, et al. Folate receptor alpha associated with triple-negative breast cancer and poor prognosis. Arch Pathol Lab Med 2014;138:890–5.
49. O'Shannessy DJ, Gustavson M, Chandrasekaran LK, Dolled-Filhart M, Somers EB. Prognostic significance of FRA expression in epithelial cancers using AQUA((R)) technology. Biomark Med 2013;7:933–46.
50. Toffoli G, Russo A, Gallo A, Cernigoi C, Miotti S, Sorio R, et al. Expression of folate binding protein as a prognostic factor for response to platinum-containing chemotherapy and survival in human ovarian cancer. Int J Cancer 1998;79:121–6.
51. Kurosaki A, Hasegawa K, Kato T, Abe K, Hanaoka T, Miyara A, et al. Serum folate receptor alpha as a biomarker for ovarian cancer: Implications for diagnosis, prognosis and predicting its local tumor expression. Int J Cancer 2016;138:1994–2002.